ACS OMEGA

http://pubs.acs.org/journal/acsodf

Article

Copper Recovery from Industrial Bimetallic Composite Ionic Liquids by Direct Electrodeposition and the Effect of Temperature and Ultrasound

Ping Ouyang, Rui Zhang, Jian Zhou, Haiyan Liu, Zhichang Liu, Chunming Xu, Xiangping Zhang, Shaojuan Zeng, Qian Su, and Xianghai Meng*

Cite This: *ACS Omega* 2023, 8, 11941−11951

Read Online

ACCESS | Metrics & More | Article Recommendations | Supporting Information

ABSTRACT: Critical processing protocols of industrial bimetallic composite ionic liquid (IL) are necessary to assure good mass transfer rates for process optimization and efficient metal recovery. Here, the effects of different conditions on the electrochemical behavior and copper recovery from the industrial bimetallic composite IL are crucial for effective resource utilization. Cyclic voltammetry (CV) shows that the reduction of Cu(I) to Cu(0) during the cathodic reduction region is the irreversible diffusion-controlled process, and the diffusion coefficient increased with temperature which indicated that increasing temperature could promote the diffusion and mass transfer. During electrodeposition, metallic copper is obtained exclusively on the cathode, while $CuCl_2$ accumulates exclusively on the anode. Scanning electron microscopy shows that the micron-size electrodeposits become larger and significantly rougher with increasing temperature and ultrasonic frequency, illustrating that these factors hasten the nucleation and crystallization rates at high overpotentials. The efficiency of copper recovery is greatly improved by employing high temperature and ultrasonic cavitation, and the highest values correspond to r = 76.9% at 80 °C and r = 63.6% at 40 kHz. The study lays the foundation for efficient and rapid recovery of copper from spent ILs.

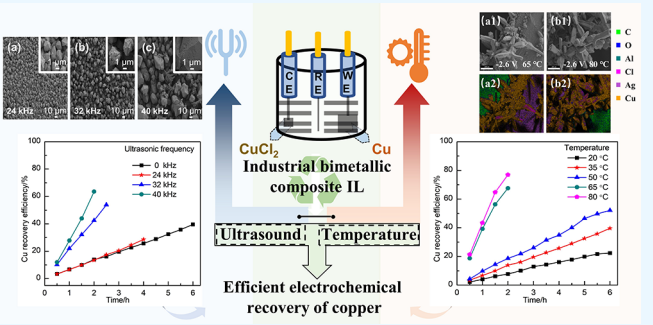

1. INTRODUCTION

Ionic liquids (ILs) have been applied in many fields and show great market potential for superiority with regard to non-volatility, thermal stability, nonflammability, structural design ability, and ionic conductivity within a wide electrochemical window.[1] ILs have been used in various industrial processes, such as the biphasic acid scavenging process of BASF to produce the generic photoinitiator precursor alkoxyphenyl-phosphines,[2,3] the Dimersol process of IFP (Institut Français du Pétrole) to provide more valuable branched hexenes and octenes,[4] the hydrosilylation process of Degussa that produces organosilicon compounds,[5,6] and composite ILs catalyzed isobutane alkylation (CILA) of China University of Petroleum-Beijing to produce alkylates.[7,8] Isobutane alkylation is one of the key processes in the production of clean gasoline; thus, the development of environmentally friendly CILA has been a major focus of the oil refining industry. Our research group has paid much attention to the development of composite IL, from basic research to pilot trials, and successively upgraded to finally realize industrial scale application. The first industrial plant of CILA successfully managed a scale of 100 kt/a output in a commercial start-up beginning in 2013. This was followed by achieving a 150 kt/a industrial output in 2018 and a 300 kt/a output in 2019. With the expansion of cooperative arrangements, there are now many plants in operation having over 1200 kt/a output of alkylate.[9−11] Bimetallic composite IL with the bimetallic center was developed on the basis of chloroaluminate-based IL, and the regeneration of Al-Cu bimetallic composite IL has been realized by the combined addition of HCl, CuCl, and $AlCl_3$ to the process,[12] but it is inevitable that spent IL accumulate in these processes and need to be discharged with lower toxicity during the course of industrial production. Subsequent treatment and recovery of spent bimetallic composite IL have become an urgent problem to be solved for these industries.

Generally, the treatment methods for ILs involve regeneration,[13,14] recovery,[15,16] and degradation[17,18] that are not generally applicable for bimetallic composite IL with complicated compositions. Based on the fact that ILs are

Received: November 28, 2022
Accepted: March 9, 2023
Published: March 22, 2023

also being proposed as alternative solution strategies for electrochemical applications such as novel electrolytes for electrodeposition, they benefit from the advantage of needing no additives. They also demonstrate high current efficiency and pose fewer environmental hazards than conventional recycling processes.[19−21] Therefore, electrodeposition provides a competitive choice for the recycling of copper resources from spent bimetallic composite IL, making waste collection profitable with low cost.

Copper has been widely applied in electrical engineering and electronic fields, especially in printed circuit board devices;[22,23] thus, the consumption of copper around the world is huge, and the market share in China accounts for more than 50% of this figure. Furthermore, with the depletion of resources and the increase of mining costs, it is important to explore the reuse of recycled copper goods, especially from industrial waste.[24,25] Recycling copper from waste will reduce pollution, so it is conducive to carbon neutrality and development of green and sustainable industries. Thermometallurgy and hydrometallurgy are commonly mentioned in the processes that regenerate and recover waste copper, and the latter are more diversified and practical, involving leaching, solvent extraction, electrolysis, electrodeposition, and chemical separation.[26] Owing to the reason that electrolytic refining of copper greatly reduces the impurity content, converts the impure copper anode to a pure copper cathode,[27] and greatly improves the economic value of waste copper. Therefore, it has become an indispensable process in copper reclamation. In addition to electrolytic refining, copper electrodeposition is also one of the effective processes that enable efficient utilization of copper resources.[28] There are many kinds of copper plating electrolytes that are commonly used in practical applications, including sulfate copper plating, cyanide copper plating, and pyrophosphate copper plating. However, traditional copper plating electrolytes are beset with problems, such as strong corrosivity, serious environmental hazards, and difficult follow-on remedies.[29] Therefore, the development of ILs for use as novel electrolytes of copper electrodeposition has become an important path for efficient resource utilization.

In developing ILs for copper electrodeposition, the recovery of copper with high efficiency and low cost is of the topmost priority. There are multi-factors affecting the electrodeposition process, such as current density,[30] potential,[31,32] stirring requirements,[33,34] temperature,[35,36] substrate material,[37] and current waveforms.[38] In addition, multi-objective research is also necessary for efficient metal recovery, and it can be realized by introducing computational fluid dynamics (CFD) simulation for developing models of metal electrodeposition[39] or response surface methodology (RSM) for the optimization of the operation parameters.[40] Therefore, it is vital to understand the effects of different factors on the electrodeposition of bimetallic composite IL so as to provide guidance for condition optimization. Industrial bimetallic composite IL was selected due to its consistency in copper electrodeposition and the superiority of quantitative analysis by inductively coupled plasma-optical emission spectroscopy (ICP-OES). Many factors are considered in laying the foundation for commercial scale-up that point the direction for efficient copper recovery from spent IL.

In this study, the effects of temperature on the electrochemical behavior of industrial bimetallic composite IL were investigated. Combining Faraday's law with the mechanism of copper electrodeposition, we establish a novel method for calculating copper recovery yield that is found suitable for bimetallic composite IL. Temperature and ultrasonic frequency were selected as important factors to explore for elevating the Cu metal yield, while maximizing the current efficiency. At the same time, the superior control over crystal morphology of solid electrodeposits is achievable. These in-depth explorations provide guidance for efficient and rapid recovery of copper from spent ILs and that is consistent with utilization of modest materials and energy resources.

2. EXPERIMENTAL SECTION

2.1. Chemicals and Reagents. All chemicals and reagents were analytical grade with purity above 99.5%. Triethylamine hydrochloride (Et_3NHCl), anhydrous aluminum chloride ($AlCl_3$), cuprous chloride (CuCl), and copper chloride ($CuCl_2$) were purchased from Aladdin. Ethanol, acetone, hydrochloric acid, nitric acid, and sulfuric acid were purchased from Innochem.

2.2. Synthesis of Bimetallic Composite IL. The synthesis procedure of bimetallic composite IL was as follows.[41] First, Et_3NHCl was added to a three-necked flask which was placed in an oil bath under stirring, with the protection of a N_2 atmosphere. A small amount of *n*-heptane was added to promote the dissolution of salts. Then, anhydrous $AlCl_3$ was added slowly in batches, and the stirred mixture was heated to 120 °C and then maintained for 2 h. Finally, CuCl was added in batches to yield a theoretical molar ratio of Et_3NHCl-2.0$AlCl_3$-0.5CuCl. The stirred mixture was then heated to 150 °C and maintained for 4 h. After standing and cooling, trace amounts of undissolved particles were filtered out and the liquid phase (IL) was stored in a glovebox. The homogeneous bimetallic composite IL was used as an electrolyte without any further treatment.

2.3. Electrochemical Measurements. Two kinds of electrochemical experiments, cyclic voltammetry measurement and electrodeposition, were carried out using an electrochemical workstation (CHI 760E, CH Instrument) in a three-electrode cell. For cyclic voltammetry, a platinum foil (10 mm × 10 mm × 0.1 mm), platinum wire (1 mm diameter), and a platinum disc electrode (exposed area of 0.071 cm^2) were used as the counter electrode, pseudo reference electrode, and working electrode, respectively. Prior to use, electrodes including platinum wire, platinum foil, and platinum plate were polished with emery paper and sequentially cleaned with acetone, dilute hydrochloric acid−sulfuric acid mixture, and deionized water. They were finally dried under a stream of N_2 gas. The CV curve was programmed to sweep from the positive potential to the negative potential, then scanned in the opposite direction after reaching a set potential, and finally stopped scanning when it reached the starting point again. The scanning rate varied between 100 and 600 $mV{\cdot}s^{-1}$. Cyclic voltammograms were obtained at different temperatures (20, 35, 50, 65, and 80 °C) and at a scanning rate of 100 $mV{\cdot}s^{-1}$. For electrodeposition, the counter electrode and pseudo reference electrode were the same as those of CV, while metal substrate copper foil (20 mm × 10 mm × 0.1 mm), nickel foil (20 mm × 10 mm × 0.1 mm), stainless steel foil (20 mm × 10 mm × 0.1 mm), zinc foil (20 mm × 10 mm × 0.1 mm), and silver foil (20 mm × 10 mm × 0.1 mm) were selected as the working electrode to determine a more suitable substrate for copper recovery. For potentiostatic electrodeposition, the conditions were as follows, the distance between the counter electrode and working electrode was 2

https://doi.org/10.1021/acsomega.2c07603
ACS Omega 2023, 8, 11941−11951

cm, the time interval was 0.5 h, temperatures were 20, 35, 50, 65, and 80 °C, and ultrasonic frequencies were 24, 32, and 40 kHz. The deposits were washed by acetone−ethanol mixed solution, then dried under a N_2 stream.

2.4. Characterization Techniques. The surface and edge morphology of the substrate were examined by scanning electron microscopy (SEM) (Carl Zeiss GeminiSEM 300), and the element composition was investigated by an X-ray energy dispersive analysis system (Horiba EMAX). The crystal phase of electrodeposits was recorded at room temperature by a Bruker D8 Advance X-ray diffractometer (Bruker AXS GmbH) with Cu Kα radiation. Anodic deposits were analyzed by a K-ALPHA X-ray photoelectron spectrometer (Thermo Scientific) with Al Kα radiation (1253.6 eV), and XPS spectra were measured with 200 eV pass energy for the survey scan and 50 eV pass energy for the scans of C 1*s*, O 1*s*, Cu 2*p*, and Cl 2*p*. UV−Vis optical absorption spectra were measured on a Cary 60 spectrophotometer, from 800 to 200 nm in 1 mm quartz cuvettes and diluted to an appropriate concentration with ethanol as the solvent. Infrared spectra were recorded by a Tensor II series FT IR spectrometer (Bruker), from 3600 to 400 cm^{-1} with a resolution of 4 cm^{-1} in 32 scans. The content of copper in the electrolyte was determined (during the long-term electrodeposition at different temperatures and different ultrasonic frequencies) using an inductively coupled plasma-optical emission spectrometer (OPTIMA7000DV, PerkinElmer). The samples were first digested with dilute nitric acid (2 wt %) and filtered after they were completely dissolved. Filtrates were diluted with deionized water to the ppm level and finally analyzed by ICP-OES.

3. RESULTS AND DISCUSSION

3.1. Effects of Temperature on Electrochemical Behavior. Figure 1a shows the cyclic voltammograms of

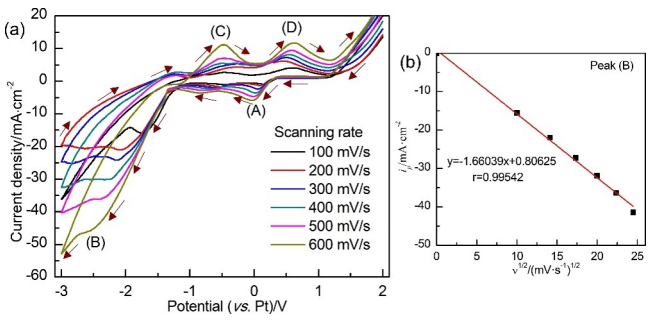

Figure 1. (a) Cyclic voltammograms of industrial bimetallic composite IL on the platinum electrode at different scanning rates and 20 °C and (b) relationship of i_p and $\nu^{1/2}$ of the cathodic peak (B).

industrial bimetallic composite IL on the platinum electrode at different scanning rates. It was apparent that the cathodic reduction of bimetallic composite IL with Cu(I) content of 5.33 wt % (1.12 mol·L^{-1}) included peak (A) and (B) that correspond to the Cu underpotential deposition (UPD) and the reduction of Cu(I) to Cu(0), respectively.[42] The anodic oxidation process included peaks (C) and (D), and they were related to Cu(0) → Cu(I) and Cu(I) → Cu(II) two-step one-electron transfer processes.[43]

The data of the CV curve for bimetallic composite IL at different scanning rates are shown in Table 1; the cathodic peak B is located between −1.75 and −2.54 V vs Pt, thus the cathodic region between −2.54 and −3.00 V for bimetallic

Table 1. Cyclic Voltammetric Data of Industrial Bimetallic Composite IL at Different Scanning Rates

	cathodic peak (E_{pc})/V vs Pt		anodic peak (E_{pa})/V vs Pt	
scanning rate (ν)/mV·s^{-1}	A	B	C	D
100	0.17	−1.75	−0.46	0.61
200	0.09	−2.09	−0.35	0.45
300	0.05	−2.12	−0.29	0.50
400	0.01	−2.27	−0.34	0.54
500	−0.02	−2.39	−0.49	0.58
600	−0.04	−2.54	−0.47	0.62

composite IL with a scanning rate of 100 mV·s^{-1} was related to the Cu overpotential deposition (OPD). Due to the huge difference in Cu(I) concentration between industrial bimetallic composite IL (mol level) and most other lower Cu(I)-containing chloroaluminate ILs (mmol level),[32,34,42−44] there was no reduction peak of Cu(II) → Cu(I). According to our study on bimetallic composite IL with different Cu(I) contents, it was found that the reduction peak of Cu(II) → Cu(I) in the CV curve was already very weak when the content of Cu(I) was 3.95 wt %. Similarly, there was no redox of aluminum in the CV curve of industrial bimetallic composite IL. It was found that only when the content of Cu(I) was reduced to 0.60 wt %, it was possible to obtain metallic aluminum at −2.6 V.[45] As shown in Figure S1, the copper content of industrial bimetallic composite IL decreased, while the aluminum content increased with time during the long-term electrodeposition at −2.6 V. This evidence should suffice to confirm the interpretation that there were only the redox of copper but not aluminum for industrial bimetallic composite IL, as shown in Figure 1a. Upon increasing the scanning rate, the current density of the UPD peak and the reduction peak of Cu(I) to Cu(0) also increased, and the corresponding peak shifted negatively, indicating that both peaks were due to irreversible reaction processes. The relationship between the current peak density i_p and the square root of scanning rate $\nu^{1/2}$ for the reduction of Cu(I) to Cu(0) (peak (B)) was plotted to see if they follow the Randles−Sevčik equation (eq 1).[29] As is shown in Figure 1b, it was clear that i_p of peak (B) showed a good linear relationship with $\nu^{1/2}$, with a correlation coefficient of 0.99542. This was interpreted to reveal that the reduction of Cu(I) to Cu(0) was a diffusion-controlled process.

$$i_p = 0.4463 \frac{n^{3/2} F^{3/2}}{R^{1/2} T^{1/2}} A c D_0^{1/2} \nu^{1/2} \quad (1)$$

Here i_p, n, F, A, c, R, T, D_0, and ν refer to the peak current, the number of moles of electrons, the Faraday constant, the area of the working electrode, the concentration of Cu(I), the gas constant, the temperature of the electrolyte, the diffusion coefficient, and the scanning rate, respectively.

As is shown in Figure 2, the current density associated with cathodic peak (B) for the reduction of Cu(I) to Cu(0) increased with temperature, and the current density at equivalent potentials also increased with temperature. According to eq 1, the diffusion coefficient (D_0) for the reduction of Cu(I) to Cu(0) at different temperatures was obtained. As shown in Table 2, the calculated values of D_0 were 9.24×10^{-7} $cm^2 \cdot s^{-1}$ at 20 °C, 2.37×10^{-6} $cm^2 \cdot s^{-1}$ at 35 °C, 3.17×10^{-6} $cm^2 \cdot s^{-1}$ at 50 °C, 1.22×10^{-5} $cm^2 \cdot s^{-1}$ at 65 °C, and 3.92×10^{-5} $cm^2 \cdot s^{-1}$ at 80 °C. The effect of temperature on the

https://doi.org/10.1021/acsomega.2c07603
ACS Omega 2023, 8, 11941−11951

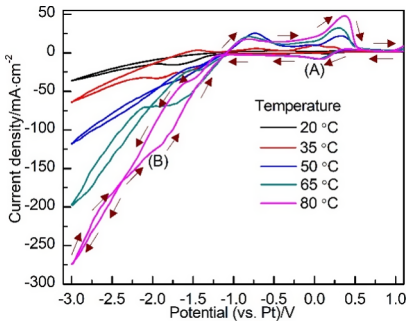

Figure 2. Cyclic voltammograms of industrial bimetallic composite IL on the platinum electrode at increasing temperatures and a scanning rate of 100 mV·s^{-1}.

Table 2. Diffusion Coefficient of Industrial Bimetallic Composite IL at Different Temperatures

temperature/°C	current density of peak B (i_p)/mA·cm^{-2}	diffusion coefficient (D_0)/cm^2·s^{-1}
20	20.99	9.24 × 10−7
35	32.80	2.37 × 10−6
50	37.04	3.17 × 10−6
65	71.01	1.22 × 10−5
80	124.51	3.92 × 10−5

diffusion coefficient was similar to that of CuCl (15 mmol) in choline chloride-ethylene glycol (ChCl-EG) deep eutectic solvent (DES), when the temperature of DES increased from 25 to 80 °C, the corresponding diffusion coefficient was increased by 5 times, that was from 3.35 × 10^{-7} to 2.31 × 10^{-6} cm^2·s^{-1}.[34] However, the diffusion coefficient of industrial bimetallic composite IL at 80 °C was about 16 times greater than that at 35 °C, thus confirming that raising the temperature promotes the diffusion and mass transfer within industrial bimetallic composite IL with a higher Cu(I) concentration of 1.12 mol·L^{-1}. In addition, cross-over behavior of the cathodic and anodic current occurred when the temperature rose above 50 °C, which indicated that a typical loop of nucleation appeared. It was particularly obvious when the temperature was elevated to 80 °C. This feature was consistent with the current loop of Cu(I) (19.58 mmol) in [Emim]BF_4 (1-ethyl-3-methylimidazolium tetrafluoroborate) IL[44] and Cu(I) (50 mmol) at 70 °C in [Bmim]SAL (1-butyl-3-methylimidazolium salicylate) IL.[32] The current loops in all cases indicated that the reduction processes at high temperatures were related to the overpotential-driven nucleation process.

3.2. Reaction Mechanism of Industrial Bimetallic Composite IL. Cu(I) ions are stable before electrochemical treatment for Cu(I)-containing ILs;[46] thus, Cu(I) species in industrial bimetallic composite IL maintain the high selectivity for isobutene alkylation.[10] As shown in Figure 3, there was a charge transfer band at 231.0 nm for both CuCl and industrial bimetallic composite IL before and after electrodeposition, indicating that there was only Cu(I) species present in industrial bimetallic composite IL during electrodeposition, and it also explained that the rationality of the reduction process of Cu(II) did not appear in the CV curve of Figure 1. On the other hand, there was a charge transfer band at 261.6 nm for both $CuCl_2$ and anodic deposits obtained from industrial bimetallic composite IL, which suggested that the anodic deposits contain Cu(II).

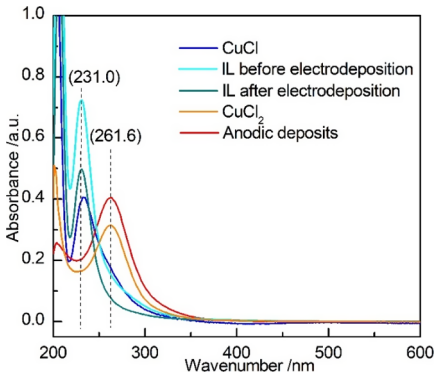

Figure 3. UV−vis spectra of CuCl, $CuCl_2$, anodic deposits, and industrial bimetallic composite IL before and after electrodeposition.

The electrodeposition mechanism of industrial bimetallic composite IL was almost the same as that of bimetallic composite ILs with a high Cu(I) content (2.23 wt %). As is shown in Figure 4a, the XRD patterns of cathodic deposits obtained at −2.6 V and 35 °C were in good agreement with the copper diffraction peaks (JCPDS Nos. 89-2838). In Figure 4b, anodic deposits were in the solid state which corresponded to the diffraction peaks of $CuCl_2(H_2O)_2$ (JCPDS Nos. 89-1697). The formation of hydrates in anodic deposits may arise from the hygroscopic propensity of $CuCl_2$ in air. As shown in Figure 4c−f, the C, Cl, O, and Cu elements are shown in XPS spectra from anodic deposits. The C 1*s* configuration was formed by the addition of carbon to the surface of deposits to increase their conductivity. The XPS spectra showed an electron emission peak at 198.6 eV that was attributed to the Cl 2*p* electron configuration. The XPS spectrum also showed two intense peaks at 933.1 and 952.8 eV which were assigned to Cu $2p_{3/2}$ and Cu $2p_{1/2}$ electrons, respectively. The Cu XPS signals were characteristic of anodic deposits and located at nearly the same energies as those of Cu(II),[47] which also confirmed that anodic copper existed in the form of $CuCl_2$.

The nonspontaneous disproportionation reaction occurred during the electrodeposition when the concentration of Cu(I) in bimetallic composite IL was higher than 0.60 wt %.[45] The disproportionation reaction was presented as Cu(I) → Cu(II) + Cu(0) in which Cu(II) species are generally present in the form of anions.[48,49] However, the generation of CuX_2 (X represents halogen) was possible under certain conditions, such as the solvent composition or the concentration of the ligand. For example, rapid disproportionation of CuBr was found to generate $CuBr_2$ and Cu in dimethyl sulfoxide (DMSO) when hexamethylated tris(2-aminoethyl)amine (Me_6-TREN) was added as the ligand.[50] Due to the low concentration of Cu(I) and ligands, it was discovered that only copper was electrodeposited on the cathode.[32,34,42−44] The high concentration of Cl^- in the present industrial bimetallic composite IL promoted the formation of $CuCl_2$. Therefore, as presented in eqs 2 and 3, metallic copper was obtained on the cathode, and high-purity $CuCl_2$ was obtained on the anode. Since both metal copper and $CuCl_2$ are useful, valuable, and recoverable products, the efficiency of copper recovery must take into consideration both the anodic and cathodic products.

$$\text{On the cathode, } [CuCl_2]^- + e^- \rightarrow Cu(s) + 2Cl^- \quad (2)$$

$$\text{On the anode, } [CuCl_2]^- \rightarrow CuCl_2(s) + e^- \quad (3)$$

https://doi.org/10.1021/acsomega.2c07603
ACS Omega 2023, 8, 11941−11951

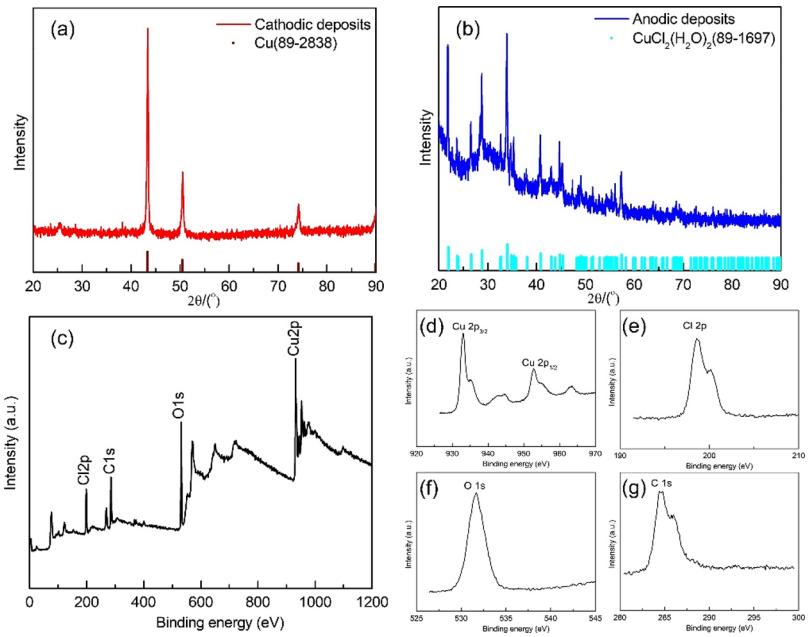

Figure 4. XRD patterns of (a) cathodic deposits and (b) anodic deposits from industrial bimetallic composite IL held on the silver foil at −2.6 V and 35 °C. XPS spectra of anodic deposits (c) survey scan, (d) Cu 2*p*, (e) Cl 2*p*, (f) O 1*s*, and (g) C 1*s*.

3.3. Methods for Calculation of Copper Recovery from Bimetallic Composite IL. The disproportionation reaction during electrodeposition was common for ILs with different metal ions (such as Pt(II), Au(I), Ce(II), etc.).[51−53] An especially similar example to the present was the disproportionation of GaCl that generated $GaCl_3$ and Ga in1-butyl-1-methylpyrrolidium bis(trifluoromethylsulfonyl)-amide ($[Py_{1,4}]$TFSI) IL.[54] However, a corresponding calculation and conversion for this disproportionation reaction has not been elucidated. Therefore, it is necessary to establish an applicable method that accounts for the variation of metal in this specific IL. According to Faraday's law, the theoretical electrodeposited mass ($m_{theoretical}$) is directly proportional to the charge exchanged,[55] which is presented in eq 4.

$$m_{theoretical} = \frac{M}{zF}Q \tag{4}$$

Here, $m_{theoretical}$, M, Q, z, and F refer to the theoretical electrodeposit mass, the molar weight, the total charge, the number of moles of electrons, and the Faraday constant, respectively.

The electrochemical equivalent $k = M/zF$, and its value for Cu(I) is 6.58×10^{-4} ($g{\cdot}C^{-1}$). That is, when the charge flow is Q during electrodeposition, the theoretical mass of copper for industrial bimetallic composite IL is $m_{Cuoncathode} = 6.58 \times 10^{-4}Q$. In calculating the copper recovery efficiency due to the disproportionation reaction, the $CuCl_2$ recovered from the anode should also be taken into consideration. Therefore, the theoretical mass of copper recovered in the overall electrochemical processing is twice as much as the cathode recovered yield, i.e., $m_{Cuintotal} = 1.32 \times 10^{-3}Q$.

The traditional method of weighting the substrates is not accurate enough to determine electrodeposit recoveries[56,57] since electrodeposits are easily lost by stripping from substrates due to their poor adhesion. Moreover, the stripping activity is particularly enhanced for electrodepositions at high temperatures. Therefore, it is necessary to establish an accurate and reliable method for measuring the electrodeposited yield from anodic and cathodic reactions of industrial bimetallic composite IL. Monitoring the content of metal present in the electrolyte in an off-line manner with high accuracy allows for more complete accounting than just measuring mass deposited on the cathode and anode. The measurements are performed by using ICP-OES, and they are more desirable than weighing to obtain accurate measurements of copper content. As is shown in eq 5, the actual electrodeposited copper can be calculated with the help of the copper content before and after electrodeposition in bimetallic composite IL. Electrochemical recovery efficiency of copper is presented as eq 6.

$$m_{actual} = w_n m_n - w_{n+1}m_{n+1} \tag{5}$$

$$\text{Percent recovery } r_n = \frac{w_0 m_0 - w_n m_n}{w_0 m_0} \times 100\% \tag{6}$$

Here, m_0 and w_0 refer to the total mass of bimetallic composite IL and the weight content of copper before electrodeposition; m_n and w_n refer to the total mass of bimetallic composite IL and the weight content of copper after electrodeposition at the nth time iteration of the measurement; m_{n+1} and w_{n+1} refer to the mass of bimetallic composite IL and the weight content of copper after electrodeposition at the $(n + 1)$th time iteration of the measurement.

The electrodeposition of IL is influenced by impurities; thus, side reactions (e.g. hydrogen evolution) lead to a mismatch between the actual consumed charge and the theoretical charge, and the ratio of the former and the latter is commonly referred to as the current efficiency (η), and it is expressed as eq 7.

$$\eta = \frac{m_{actual}}{m_{theoretical}} \times 100\% \tag{7}$$

Here, η, m_{actual}, and $m_{theoretical}$ refer, respectively, to the current efficiency, actual mass transferred, and theoretical mass of electrodeposits transferred, including impurities.

https://doi.org/10.1021/acsomega.2c07603
ACS Omega 2023, 8, 11941−11951

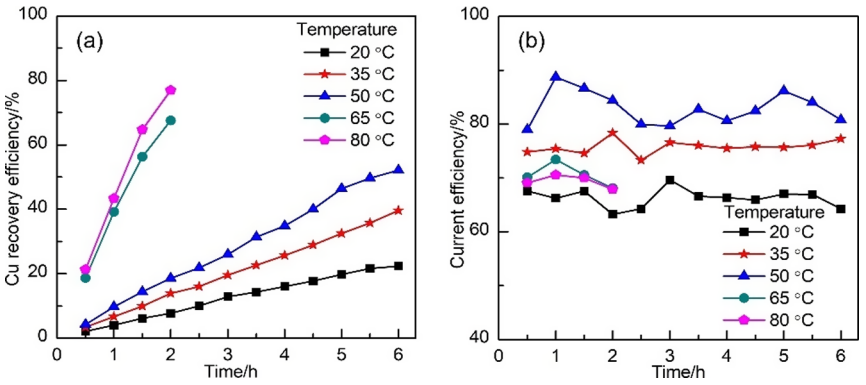

Figure 5. Effects of different temperatures (20, 35, 50, 65, and 80 °C) on (a) copper recovery efficiency and (b) current efficiency of industrial bimetallic composite IL.

3.4. Determination of Substrate and Potential for Copper Electrodeposition. According to eq 4, the theoretical mass of copper released from industrial bimetallic composite IL is related to the measured charge transferred. This suggests that many parameters affecting charge consumption should be considered in optimizing the capture and release processes. We are aware that certain operational conditions like potential, substrate, temperature, and ultrasound frequency should be considered as key factors that determine r_n and η for copper electrodeposition.

Table S1 shows the consumed charge on different substrates and Figure S2 shows the variation of charge with potential for the electrodeposition of bimetallic composite IL. While the effect of substrates was smaller than that of potentials, and the charge of silver foil was the highest among the substrates. The consumed charge at different potentials varied greatly; it increased when the potentials shifted negatively in the electrochemical window between −1.2 and −3.0 V. Because the slope is greatest between −2.2 and −2.6 V; thus, we initially selected the operating potential at −2.6 V to be a useful working potential for electrodeposition on silver foil.

3.5. Effects of Temperature on Copper Electrodeposition. The copper content in bimetallic composite IL before and after electrodeposition was determined by ICP-OES. The initial value was 5.33 wt %, and it decreased progressively with electrodeposition. Copper recovery efficiency was calculated by eq 6 and current efficiency by eq 7. As shown in Figure 5a, copper recovery efficiency gradually increased with temperature. When the electrodeposition was allowed to continue 2 h, copper recovery efficiencies at 65 and 80 °C were correspondingly 67.6 and 76.9%. The copper recovery efficiency at 80 °C were about 4 times the efficiency at 50 °C (18.6%), while the D_0 value at 80 °C was about 12 times that at 50 °C. Therefore, it became evident that the mass diffusional transfer was greatly enhanced when the temperature was raised from 50 to 80 °C. Current efficiency at different temperatures is plotted in Figure 5b. The overall current efficiency increased as temperature increased from 20 to 50 °C and then turned downward at temperatures in excess of 50 °C. The average current efficiency at 65 °C corresponded to 70.6% and 80 °C to 69.4%, both lower than that at 50 °C (82.9%). The decrease of current efficiency was due to the electrochemical degradation of triethylamine hydrochloride in the electrolyte, which is common in quaternary ammonium ILs at sufficiently negative potential.[58] As shown in Figure S3a, the peak of the C-N stretching vibration region of $(C_2H_5)_3NH^+$ cations[59] (445.5 cm^{-1}) in IR spectra blue-shifted with temperature, indicating that the structure of the cations was changed. In the case of industrial bimetallic composite IL, its electrochemical degradation is beneficial for the electrochemical treatment.

The morphology of these electrodeposits obtained at different potentials and temperatures is shown in Figure 6. For the electrodeposition at 35 °C (Figure 6b1−b3), the extent of aggregation of electrodeposits increased as the potential shifted from −1.2 V (potential region for the reduction of Cu(I)) to −2.6 V (potential region for Cu OPD), and the surface of the substrate becomes progressively rougher and the particle size smaller with the negative shift of potential. The effect of temperature on morphology was mainly followed at discrete potentials (−1.2, −1.7, and −2.6 V). For electrodeposition at −1.2 V, the morphology of electrodeposits forms rodlike copper grains at 20 °C (Figure 6a1). While they appeared fairly uniform in the size of grains at 20 °C, they gradually increased in size as the temperature increased to 35 °C and increased further in size up to 80 °C (Figure 6b1−e1). Modulating these positive changes in particle size with temperature were negative changes in particle size with the magnitude of the potential. Grain coarsening of the copper electrodeposits that was caused by the increase of temperature was similar to that seen in the ChCl-EG DES containing 0.1 mmol Cu(II).[40] The particle morphology for copper that electrodeposits at 20 °C and a potential of −1.7 V (Figure 6a2) was essentially the same morphology as that obtained at −1.2 V. While crystallites appeared somewhat more irregular in shape, and the size of aggregates did not change until the temperature was raised to 35 °C and beyond (Figure 6b2−e2). For the electrodeposition occurring at −2.6 V, the morphology of the electrodeposits in Figure 6a3 was also rodlike and similar to the copper deposited at 20 °C and −1.2 V. However, the aggregates appeared more irregular in shape and size. The size of aggregates gradually increased at −1.7 V as the temperature increased from 35 to 50 °C (Figure 6b2−c2). The electrodeposits exhibited dendritic growth as the temperature further increased to 65 °C (Figure 6d3). They remain dendritic as the temperature rose to 80 °C (Figure 6e3). It is evident that temperature has pronounced influence on the morphology and micron size of electrodeposits.

The elemental distribution of electrodeposits at high temperatures was measured by energy dispersive X-ray (EDX) element mapping, as is shown in Figure 7. The edge of silver foil that had been held at −2.6 V and 65 °C was

https://doi.org/10.1021/acsomega.2c07603
ACS Omega 2023, 8, 11941−11951

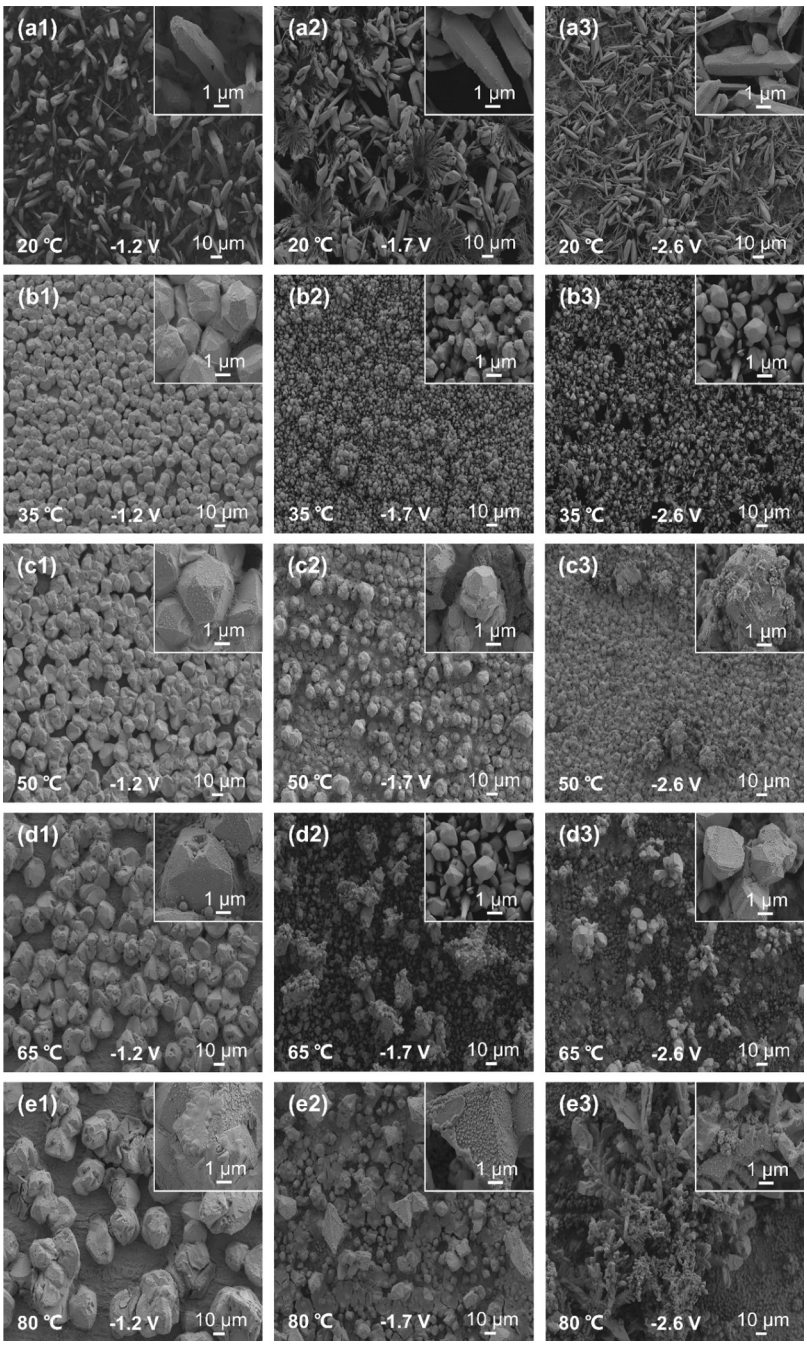

Figure 6. Effects of temperatures and potentials on the structural morphology of deposits from industrial bimetallic composite IL on the silver foil at (a) 20 °C, (b) 35 °C, (c) 50 °C, (d) 65 °C, and (e) 80 °C.

conspicuously composed of dendritic copper (Figure 7a1,a2)). The whiskers of dendrite copper grow longer and became hollow after the temperature increased to 80 °C (Figure 7b1,b2). The change of morphology may be related to rapid nucleation and crystallization at a high temperature and high overpotential,[60] as suggested by Figure 2, where the current density of the nucleation loop exhibited a marked increase in charge transfer at 65 and 80 °C.

The copper content for electrodeposits that were carried out at −2.6 V and different temperatures was obtained by EDX, as is shown in Figure S4. On increasing the deposition temperature from 20 to 80 °C in 15 °C steps, the corresponding copper contents were 96.55, 98.59, 94.79, 94.70, and 98.09 wt %. It was significant that electrodeposits basically comprise copper and little, if any, aluminum in residual IL deposition. The little Ag found in these deposits is derived from substrate interference. On the basis of this analysis, we extracted samples and identified the principal reflecting planes of XRD patterns of electrodeposits produced at −2.6 V and different temperatures, as shown in Figure 8. All electrodeposits were consistent with the copper diffraction peaks (JCPDS Nos. 89-2838) containing Cu(111), Cu(200), Cu(220), and Cu(311) peaks corresponding to 2 theta angles of 43.31, 50.45, 74.12, and 89.93°. The data indicated that the electrodeposits at different temperatures were of metallic copper, but the peak intensity of Cu(111) markedly increased with temperature.

https://doi.org/10.1021/acsomega.2c07603
ACS Omega 2023, 8, 11941−11951

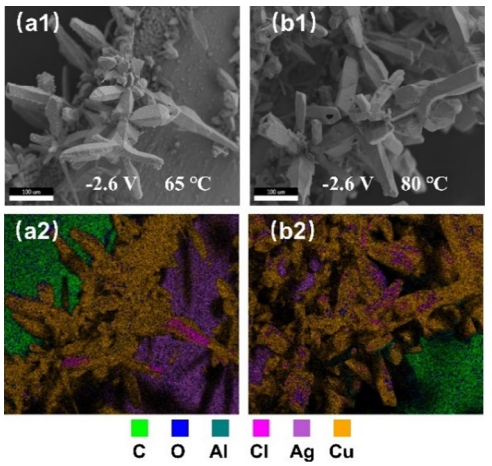

Figure 7. SEM images and overlap with EDX element mapping of electrodeposits on the edge of the silver foil electrode that was held at −2.6 V from industrial bimetallic composite IL at (a) 65 °C and (b) 80 °C.

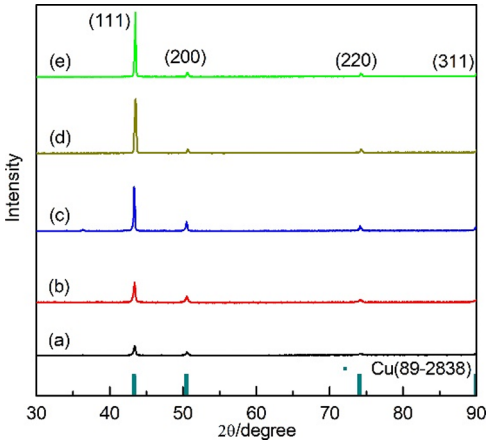

Figure 8. XRD pattern of electrodeposits at −2.6 V from industrial bimetallic composite IL at (a) 20 °C, (b) 35 °C, (c) 50 °C, (d) 65 °C, and (e) 80 °C.

3.6. Effects of Ultrasound Frequency on Copper Electrodeposition. Due to cavitation processes of ultrasound-driven fluids, trapped gas bubbles accelerate IL fluid movement and raise its turbulence. Raising the ultrasonic frequency produces smaller, more copious gas bubbles that further increase turbulence and accelerate mixing rates.[61] Therefore, different ultrasonic frequency was selected to further explore the effect on electrochemical recovery of copper from the bimetallic composite IL. As shown in Figure 9, the efficiency of copper recovery greatly improved on raising the ultrasonic frequency. The efficiency of copper recovery reached 63.6% in 2 h at 35 °C and 40 kHz. This recovery efficiency was much greater than that achieved under the same conditions without ultrasound (13.9%). At the same time, the current efficiency diminished as the ultrasonic frequency was raised from 0 to 40 kHz. The average current efficiency of 40 kHz at 35 °C was 51.8%, which was lower than that at 35 °C without ultrasound (75.8%). As is shown in Figure S3b, the peak of the C-N stretching vibration region of $(C_2H_5)_3NH^+$ cations (446.9 cm^{-1}) also blueshifted with the increase of ultrasonic frequencies, indicating that the structure of the cations was changed. Thus, the decrease of current efficiency was also related to the electrochemical degradation of triethylamine hydrochloride.

The SEM images of samples deposited at −2.6 V are presented in Figure 10 showing copper grains collected at different ultrasonic frequencies. The uniform size of grains on the silver foil became larger and significantly rougher as the ultrasonic frequency increased from 24 to 40 kHz, indicating that ultrasound is useful to obtain coarse and large grains. The copper content in the grains deposited under these conditions was measured by EDX, as is shown in Figure S5. When the ultrasonic frequencies were varied, their copper contents were measured to be 97.07, 98.10, and 95.80 wt % corresponding to 24, 32, and 40 kHz, which indicates that the electrodeposits were composed primarily of copper, with very little, if any aluminum present.

4. CONCLUSIONS

Effects of temperature and ultrasound on the electrochemical behavior and electrochemical recovery of copper were investigated. The cyclic voltammograms of industrial bimetallic composite IL at different temperatures and scanning rates were measured. The cathodic reduction processes included the Cu UPD, the reduction of Cu(I) to Cu(0), and Cu OPD. The reduction of Cu(I) to Cu(0) was an irreversible diffusion-controlled process, and the diffusion coefficient increased with temperature, indicating that increasing temperature could promote diffusion and mass transfer. There was a typical loop of nucleation in the CV curve when the temperature rose to 50 °C and above, revealing that the reduction process involved an overpotential-driven nucleation process. Based on

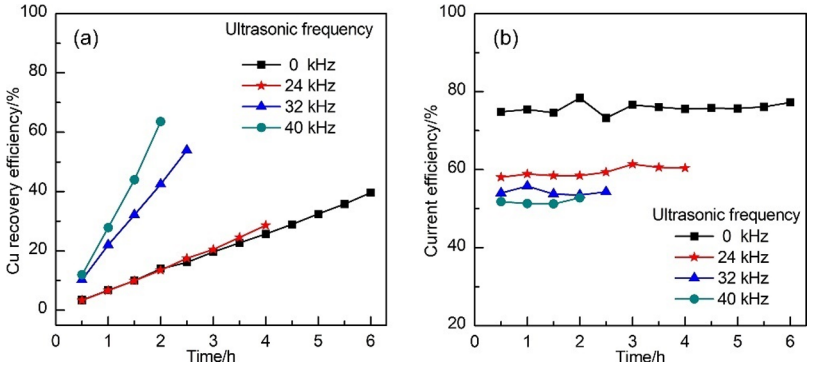

Figure 9. Effects of different ultrasonic frequencies (0, 24, 32, and 40 kHz) on (a) copper recovery efficiency and (b) current efficiency from industrial bimetallic composite IL at 35 °C.

https://doi.org/10.1021/acsomega.2c07603
ACS Omega 2023, 8, 11941−11951

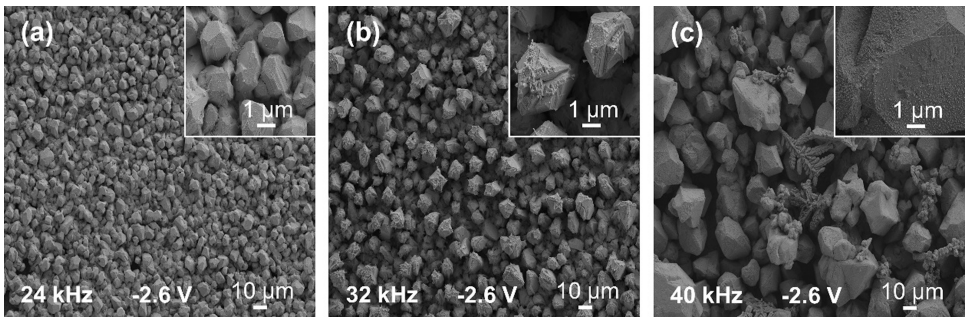

Figure 10. Effects of ultrasonic frequency on the morphology of deposits from industrial bimetallic composite IL on the silver foil at −2.6 V, 35 °C and (a) 24 kHz, (b) 32 kHz, and (c) 40 kHz.

the disproportionation of Cu(I), metallic copper and $CuCl_2$ were obtained on the cathode and the anode, respectively. By combining Faraday's law and mass balance during copper electrodeposition that accounts for both anodic and cathodic products, a novel quantitative method for calculating copper recovery was established. Temperature and ultrasound were selected as key factors to investigate their influence upon copper recovery and current efficiency. It was found that copper recovery increased with increasing temperatures (r = 76.9% at 80 °C and 0 kHz) or ultrasonic frequency (r = 63.6% at 35 °C and 40 kHz). On the other hand, current efficiency first increased, then decreased with temperature, and decreased monotonically as the ultrasonic frequency increased. SEM of electrodeposits at different potentials show a roughening of surface features that become rougher as the potential negatively shifts. The grain size of the electrodeposits become larger with increasing temperature or ultrasonic frequency. Although thermal effects are more effective than that of ultrasound, it is believed that a combination of both will raise promising synergistic enhancements for greater efficiency. In addition, there is still a long way to go for the scale-up process. Many techniques like thermodynamic study, RSM, and CFD simulation can also provide supports for the optimization of the operation parameters, comprehensive design of the metal recycling strategy, and efficient resource utilization for other metal-containing ILs.

■ ASSOCIATED CONTENT

Supporting Information

The Supporting Information is available free of charge at https://pubs.acs.org/doi/10.1021/acsomega.2c07603.

Charge for the electrodeposition of bimetallic composite IL at 20 °C and −2.6 V on different electrode substrates; variation of the aluminum element and the copper element in industrial bimetallic composite IL at 20 °C and −2.6 V during long-term electrodeposition; variation of charge with potentials for the electrodeposition from industrial bimetallic composite IL on silver foil at 20 °C; IR spectra of industrial bimetallic composite IL before and after electrodeposition at (a) different temperatures and (b) different ultrasonic frequencies; EDX spectra of electrodeposits on silver foil at −2.6 V from industrial bimetallic composite IL at (a) 20 °C, (b) 35 °C, (c) 50 °C, (d) 65 °C, and (e) 80 °C; and EDX spectra of electrodeposits on silver foil at −2.6 V from industrial bimetallic composite IL at (a) 24 kHz, (b) 32 kHz, and (c) 40 kHz (PDF)

■ AUTHOR INFORMATION

Corresponding Author

Xianghai Meng − *State Key Laboratory of Heavy Oil Processing, China University of Petroleum, Beijing 102249, China;* orcid.org/0000-0001-9494-6996; Email: mengxh@cup.edu.cn

Authors

Ping Ouyang − *State Key Laboratory of Heavy Oil Processing, China University of Petroleum, Beijing 102249, China*

Rui Zhang − *State Key Laboratory of Heavy Oil Processing, China University of Petroleum, Beijing 102249, China*

Jian Zhou − *State Key Laboratory of Heavy Oil Processing, China University of Petroleum, Beijing 102249, China*

Haiyan Liu − *State Key Laboratory of Heavy Oil Processing, China University of Petroleum, Beijing 102249, China*

Zhichang Liu − *State Key Laboratory of Heavy Oil Processing, China University of Petroleum, Beijing 102249, China*

Chunming Xu − *State Key Laboratory of Heavy Oil Processing, China University of Petroleum, Beijing 102249, China*

Xiangping Zhang − *State Key Laboratory of Heavy Oil Processing, China University of Petroleum, Beijing 102249, China;* orcid.org/0000-0002-1431-0873

Shaojuan Zeng − *State Key Laboratory of Multiphase Complex System, Beijing Key Laboratory of Ionic Liquids Clean Process, Institute of Process Engineering, Chinese Academy of Sciences, Beijing 100190, China;* orcid.org/0000-0002-0070-6711

Qian Su − *State Key Laboratory of Multiphase Complex System, Beijing Key Laboratory of Ionic Liquids Clean Process, Institute of Process Engineering, Chinese Academy of Sciences, Beijing 100190, China*

Complete contact information is available at: https://pubs.acs.org/10.1021/acsomega.2c07603

Notes

The authors declare no competing financial interest.

■ ACKNOWLEDGMENTS

This work was supported by the Natural Science Foundation of China (22021004, 21890763).

■ REFERENCES

(1) Dong, K.; Liu, X.; Dong, H.; Zhang, X.; Zhang, S. Multiscale studies on ionic liquids. *Chem. Rev.* **2017**, *117*, 6636−6695.

(2) Seddon, K. R. Ionic liquids: A taste of the future. *Nat. Mater.* **2003**, *2*, 363−365.

(3) Rogers, R. D.; Seddon, K. R. Ionic liquids-solvents of the future? *Science* **2003**, *302*, 792−793.
(4) Chauvin, Y.; Gaillard, J. F.; Quang, D. V.; Andrews, K. W. The IFP dimersol process for the dimerisation of C3 and C4 olefinic cuts. *Chem. & Ind.* **1974**, 375−378.
(5) Hoff, A.; Jost, D.; Prodi-Schwab, A.; Schmidt, F. G.; Weyershausen, B. Ionic Liquids: New Designer Compounds for More Efficient Chemistry. *Elements: Degussa Sci. Newslett.* **2004**, *9*, 10−15.
(6) Weyershausen, B.; Hell, K.; Hesse, U. Industrial application of ionic liquids as process aid. *Green Chem.* **2005**, *7*, 283−287.
(7) Huang, C.; Liu, Z.; Xu, C.; Chen, B.; Liu, Y. Effects of additives on the properties of chloroaluminate ionic liquids catalyst for alkylation of isobutane and butene. *Appl. Catal. A Gen.* **2004**, *277*, 41−43.
(8) Liu, Z.; Zhang, R.; Liu, Y.; Xu, C. Study on isobutane alkylation catalyzed by composite ionic liquid. *J. Fuel Chem. Technol.* **2006**, *34*, 328−331.
(9) Liu, Z.; Meng, X.; Zhang, R.; Xu, C.; Dong, H.; Hu, Y. Reaction performance of isobutane alkylation catalyzed by a composite ionic liquid at a short contact time. *AIChE J.* **2014**, *60*, 2244−2253.
(10) Meng, X.; Zhang, R.; Liu, H.; Zhang, X.; Liu, Z.; Xu, C.; Klusener, P. A. A. Development and application of composite ionic liquid catalyzed isobutane alkylation technology. *Sci. Sin. Chim.* **2018**, *48*, 387−396.
(11) Chung, W.; Zhang, R.; Song, D. Safe and sustainable alkylation: Performance and update on composite ionic liquid alkylation technology. *Hydrocarb. Process* **2020**, *99*, 25−28.
(12) Zhang, X.; Zhang, R.; Meng, X.; Liu, H.; Liu, Z.; Ma, H.; Xu, C.; Klusener, P. A. A. Deactivation mechanism and activity-recovery approach of composite ionic liquids for isobutane alkylation. *Appl. Catal. A Gen.* **2018**, *557*, 64−71.
(13) Parmentier, D.; Valia, Y. A.; Metz, S. J.; Burheim, O. S.; Kroon, M. C. Regeneration of the ionic liquid tetraoctylammonium oleate after metal extraction. *Hydrometallurgy* **2015**, *158*, 56−60.
(14) Huang, C.; Huang, B.; Dong, Y.; Chen, J.; Wang, Y.; Sun, X. Efficient and sustainable regeneration of bifunctional ionic liquid for rare earth separation. *ACS Sustainable Chem. Eng.* **2017**, *5*, 3471−3477.
(15) Bai, L.; Wang, X.; Nie, Y.; Dong, H.; Zhang, X.; Zhang, S. Study on the recovery of ionic liquids from dilute effluent by electrodialysis method and the fouling of cation-exchange membrane. *Sci. China Chem.* **2013**, *56*, 1811−1816.
(16) Wong, H.; Pink, C. J.; Ferreira, F. C.; Livingston, A. G. Recovery and reuse of ionic liquids and palladium catalyst for Suzuki reactions using organic solvent nanofiltration. *Green Chem.* **2006**, *8*, 373−379.
(17) Ren, T.; Ma, X.; Wu, X.; Yuan, L.; Lai, Y.; Tong, Z. Degradation of imidazolium ionic liquids in a thermally activated persulfate system. *Chem. Eng. J.* **2021**, *412*, No. 128624.
(18) Zhou, H.; Shen, Y.; Lv, P.; Wang, J.; Fan, J. Degradation of 1-butyl-3-methylimidazolium chloride ionic liquid by ultrasound and zero-valent iron/activated carbon. *Sep. Purif. Technol.* **2013**, *104*, 208−213.
(19) Barrado, E.; Rodriguez, J. A.; Hernández, P.; Castrillejo, P. Electrochemical behavior of copper species in the 1-buthyl-3-methyl-imidazolium chloride (BMIMCl) ionic liquid on a Pt electrode. *J. Electroanal. Chem.* **2016**, *768*, 89−101.
(20) Nanjundiah, C.; Osteryoung, R. A. Electrochemical studies of Cu(I) and Cu(II) in an aluminum chloride-N-(N-Butyl) Pyridinium chloride ionic liquid. *J. Electrochem. Soc.* **1983**, *130*, 1312−1318.
(21) El Abedin, S. Z.; Pölleth, M.; Meiss, S. A.; Janek, J.; Endres, F. Ionic liquids as green electrolytes for the electrodeposition of nanomaterials. *Green Chem.* **2007**, *9*, 549−553.
(22) Iglesias-González, N.; Carranza, F.; Mazuelos, A.; Romero, R.; Lorenzo-Tallafigo, J.; Romero-García, A.; Ramírez, P. The BRISA process as a path for efficient copper recovery from waste PCBs. *Hydrometallurgy* **2021**, *205*, No. 105750.
(23) Barragan, J. A.; Ponce de León, C.; Alemán Castro, J. R.; Peregrina-Lucano, A.; Gómez-Zamudio, F.; Larios-Durán, E. R. Copper and antimony recovery from electronic waste by hydro-metallurgical and electrochemical techniques. *ACS Omega* **2020**, *5*, 12355−12363.
(24) Lee, J.; Kurniawan, K.; Chung, K. W.; Kim, S. Metallurgical process for total recovery of all constituent metals from copper anode slimes: A review of established technologies and current progress. *Met. Mater. Int.* **2021**, *27*, 2160−2187.
(25) Lei, T.; Shu, J.; Deng, Y.; Hu, L.; Chen, S.; Chen, M.; Huang, W. Enhanced recovery of copper from reclaimed copper smelting fly ash via leaching and electrowinning processes. *Sep. Purif. Technol.* **2021**, *273*, No. 118943.
(26) Vukmirovic, M. B.; Adzic, R. R.; Akolkar, R. Copper electrodeposition from deep eutectic solvents-voltammetric studies providing insights into the role of substrate: platinum vs glassy Carbon. *J. Phys. Chem. B* **2020**, *124*, 5465−5475.
(27) Shi, M.; Min, X.; Chen, S.; Chai, L.; Ke, Y.; Yan, X.; Liang, Y. Separation and recovery of copper in Cu-As-bearing copper electrorefining black slime by oxidation acid leaching and sulfide precipitation. *Trans. Nonferr. Metal. Soc. China* **2021**, *31*, 1103−1112.
(28) Jin, W.; Zhang, Y. Sustainable electrochemical extraction of metal resources from waste streams: from removal to recovery. *ACS Sustainable Chem. Eng.* **2020**, *8*, 4693−4707.
(29) Abbott, A. P.; El Ttaib, K.; Frisch, G.; McKenzie, K. J.; Ryder, K. S. Electrodeposition of copper composites from deep eutectic solvents based on choline chloride. *Phys. Chem. Chem. Phys.* **2009**, *11*, 4269−4277.
(30) Oliveira, J. A. M.; de Almeida, A. F.; Campos, A. R. N.; Prasad, S.; Alves, J. J. N.; de Santana, R. A. C. Effect of current density, temperature and bath pH on properties of Ni-W-Co alloys obtained by electrodeposition. *J. Alloys Compd.* **2021**, *853*, No. 157104.
(31) Chen, P. Y.; Chang, Y. T. Voltammetric study and electrodeposition of copper in 1-butyl-3-methylimidazolium salicylate ionic liquid. *Electrochim. Acta* **2012**, *75*, 339−346.
(32) Grujicic, D.; Pesic, B. Electrodeposition of copper: the nucleation mechanisms. *Electrochim. Acta* **2002**, *47*, 2901−2912.
(33) Mandroyan, A.; Mourad-Mahmoud, M.; Doche, M. L.; Hihn, J. Effects of ultrasound and temperature on copper electro reduction in deep eutectic solvents (DES). *Ultrason. Sonochem.* **2014**, *21*, 2010−2019.
(34) Choudhary, R. K.; Kain, V.; Hubli, R. C. Stirring effects on aluminium coatings electrodeposited in ionic liquids. *Surf. Eng.* **2014**, *30*, 562−567.
(35) Lv, J.; Liang, T.; Wang, C. Effect of electrodeposition temperature on grain orientation and corrosion resistance of nanocrystalline pure nickel. *J. Solid State Chem.* **2016**, *240*, 109−114.
(36) Gheitaghy, A. M.; Saffari, H.; Ghasimi, D.; Ghasemi, A. Effect of electrolyte temperature on porous electrodeposited copper for pool boiling enhancement. *Appl. Therm. Eng.* **2017**, *113*, 1097−1106.
(37) Banthia, S.; Sengupta, S.; Mallik, M.; Das, S.; Das, K. Substrate effect on electrodeposited copper morphology and crystal shapes. *Surf. Eng.* **2018**, *34*, 485−492.
(38) Xing, S.; Zanella, C.; Deflorian, F. Effect of pulse current on the electrodeposition of copper from choline chloride-ethylene glycol. *J. Solid State Electrochem.* **2014**, *18*, 1657−1663.
(39) Barragan, J. A.; Tesillo-Perales, M.; Castro, J. R. A.; Larios-Durán, E. R.; Rivero, E. P. Optimization of a rotating cylinder electrode electrochemical reactor for metal recovery: An innovative approach and method combining CFD and response surface methodology. *Electrochim. Acta* **2022**, *435*, No. 141335.
(40) Barragan, J. A.; Castro, J. R. A.; Peregrina-Lucano, A. A.; Sánchez-Amaya, M.; Rivero, E. P.; Larios-Durán, E. R. Leaching of metals from e-waste: from its thermodynamic analysis and design to its implementation and optimization. *ACS Omega* **2021**, *6*, 12063−12071.
(41) Liu, Z.; Zhang, Y.; Huang, C.; Gao, J.; Xu, C. Effect of CuCl ddditive on catalytic performance of $Et_3NHCl/AlCl_3$ ionic liquid in C4 alkylation. *Chinese J. Catal.* **2004**, *25*, 693−696.

https://doi.org/10.1021/acsomega.2c07603
ACS Omega 2023, 8, 11941−11951

(42) Endres, F.; Schweizer, A. The electrodeposition of copper on Au(111) and on HOPG from the 66/34 mol% aluminium chloride/1-butyl-3-methylimidazolium chloride room temperature molten salt: an EC-STM study. *Phys. Chem. Chem. Phys.* **2000**, *2*, 5455−5462.
(43) Assaker, I. B.; Dhahbi, M. Electrochemical study and electrodeposition of copper in the hydrophobic tri-n-octylmethylammonium chloride ionic liquid media. *J. Mol. Liq.* **2011**, *161*, 13−18.
(44) Chen, P. Y.; Sun, I. W. Electrochemical study of copper in a basic 1-ethyl-3-methylimidazolium tetrafluoroborate room temperature molten salt. *Electrochim. Acta* **1999**, *45*, 441−450.
(45) Ouyang, P.; Zhang, R.; Zhou, J.; Liu, H.; Liu, Z.; Xu, C.; Zeng, S.; Su, Q.; Zhang, X.; Meng, X. Effects of Cu(I) contents on the voltammetric behavior and electrodeposition mechanism of bimetallic composite ionic liquids. *New J. Chem.* **2022**, *46*, 16183−16191.
(46) Schaltin, S.; Brooks, N. R.; Binnemans, K.; Fransaer, J. Electrodeposition from cationic cuprous organic complexes: ionic liquids for high current density electroplating. *J. Electrochem. Soc.* **2011**, *158*, D21−D27.
(47) Dang, Y.; Cheng, Y.; Zhou, Y.; Huang, Y.; Wang, Y. Nano-PAA-$CuCl_2$ composite as Fenton-like reusable catalyst to enhanced degrade organic pollutant MB/MO. *Catalysts* **2021**, *11*, 10.
(48) Krzewska, S. Impedance investigation of the mechanism of copper electrodeposition from acidic perchlorate electrolyte. *Electrochim. Acta* **1997**, *42*, 3531−3540.
(49) Lewandowski, A. I. Ionic solvation. Part 4.-Copper(I) solvation. Disproportionation and halide-complex formation in propylene carbonate. *J. Chem. Soc Faraday Trans.* **1988**, *84*, 4013−4021.
(50) Rosen, B. M.; Jiang, X.; Wilson, C. J.; Nguyen, N. H.; Monteiro, M. J.; Percec, V. The disproportionation of Cu(I)X mediated by ligand and solvent into Cu(0) and Cu(II)X_2 and its implications for SET-LRP. *J. Polym. Sci., Part A: Polym. Chem.* **2009**, *47*, 5606−5628.
(51) Zhang, D.; Chang, W. C.; Okajima, T.; Ohsaka, T. Electrodeposition of platinum nanoparticles in a room-temperature ionic liquid. *Langmuir* **2011**, *27*, 14662−14668.
(52) Oyama, T.; Okajima, T.; Ohsaka, T. Electrodeposition of gold at glassy carbon electrodes in room-temperature ionic liquids. *J. Electrochem. Soc.* **2007**, *154*, D322−D327.
(53) Chou, L. H.; Cleland, W. E.; Hussey, C. L. Electrochemical and spectroscopic study of Ce(III) coordination in the 1-butyl-3-methylpyrrolidinium bis (trifluoromethylsulfonyl) imide ionic liquid containing chloride ion. *Inorg. Chem.* **2012**, *51*, 11450−11457.
(54) Liu, Z.; Hofft, O.; Endres, F. Disproportionation reaction of gallium during electrodeposition from an ionic liquid, monitored by in situ electrochemical XPS. *J. Phys. Chem. C* **2021**, *125*, 24589−24595.
(55) Schlesinger, M.; Paunovic, M. *Modern electroplating*; John Wiley & Sons: New York, 2010.
(56) Janin, A.; Coudert, L.; Mercier, G.; Blais, J. Copper extraction and recovery from alkaline copper quaternary and copper azole treated wood using sulfuric acid leaching and ion exchange or electrodeposition. *J. Cleaner Prod.* **2021**, *279*, No. 123687.
(57) Jin, W.; Su, J.; Zheng, S.; Lei, H. Controlled electrodeposition of uniform copper powder from hydrochloric acid solutions. *J. Electrochem. Soc.* **2017**, *164*, D723−D728.
(58) Finkelstein, M.; Petersen, R. C.; Ross, S. D. The electrochemical degradation of quaternary ammonium salts1. *J. Am. Chem. Soc.* **1959**, *81*, 2361−2364.
(59) Bednarska-Bolek, B.; Ciunik, Z.; Jakubas, R.; Bator, G.; Ciapala, P. Structure and phase transitions in chloroantimonate(V) crystals: $[(C_2H_5)_3NH]SbCl_6$ and $[(C_2H_5)_3NH]SbCl_6{\cdot}1/2[(C_2H_5)_3NH]Cl$. *J. Phys. Chem. Solids* **2002**, *63*, 507−518.
(60) Bograchev, D. A.; Davydov, A. D. Effect of applied temperature gradient on instability of template-assisted metal electrodeposition. *Electrochim. Acta* **2019**, *296*, 1049−1054.
(61) Doche, M. L.; Mandroyan, A.; Mourad-Mahmoud, M.; Moutarlier, V.; Hihn, J. An ultrasonic-assisted process for copper recovery in a des solvent: Leaching and re-deposition. *Chem. Eng. Process.* **2017**, *121*, 90−96.

https://doi.org/10.1021/acsomega.2c07603
ACS Omega 2023, 8, 11941−11951